European Journal of Nuclear Medicine and Molecular Imaging (2024) 51:2931–2940
https://doi.org/10.1007/s00259-024-06602-3

REVIEW ARTICLE

Current clinical applications of Cerenkov luminescence for intraoperative molecular imaging

Natalie Boykoff[1,2,3,4] · **Jan Grimm**[3,4,5,6]

Received: 30 August 2023 / Accepted: 4 January 2024 / Published online: 20 January 2024
© The Author(s), under exclusive licence to Springer-Verlag GmbH Germany, part of Springer Nature 2024, corrected publication 2024

Abstract

Background Cerenkov luminescence imaging (CLI) is a new emerging technology that can be used for optical imaging of approved radiotracers, both in a preclinical, and even more recently, in a clinical context with rapid imaging times, low costs, and detection in real-time (Grootendorst et al. Clin Transl Imaging 4(5):353–66, 2016); Wang et al. Photonics 9(6):390, 2022). This brief review provides an overview of clinical applications of CLI with a focus on intraoperative margin assessment (IMA) to address shortcomings and provide insight for future work in this application.

Methods A literature review was performed using PubMed using the search words Cerenkov luminescence imaging (CLI), intraoperative margin assessment (IMA), and image-guided surgery. Articles were selected based on title, abstract, content, and application.

Results Original research was summarized to examine advantages and limitations of CLI compared to other modalities for IMA. The characteristics of Cerenkov luminescence (CL) are defined, and results from relevant clinical trials are discussed. Prospects of ongoing clinical trials are reviewed, along with technological advancements related to CLI.

Conclusion CLI is a proven method for molecular imaging and shows feasibility for determining intraoperative margins if future work involves establishing quantitative approaches for attenuation and scattering, depth analysis, and radiation safety for CLI at a larger scale.

Keywords Cerenkov luminescence imaging · Intraoperative margin assessment · Image-guided surgery · Molecular imaging

Imaging modalities for intraoperative margin assessment

Approximately 80% of cancer cases between 2012 and 2030 (~ 17.3 million) are anticipated to require surgical intervention as the primary form of curative treatment [1, 2]. To achieve curative efficacy, complete tumor resection with minimal damage to normal tissue structure and function must be achieved, as only this results in higher survival rates compared to other forms of cancer therapy [3]. Ideally, surgeons aim to excise the lesion with a surrounding margin of healthy tissue (~ 5 mm), leaving in the patient a negative surgical margin (NSM), while sparing as much healthy tissue as possible before compromising oncological safety [1, 3], which in some cases excludes surgery as an option, e.g., when the tumor directly impacts vital tissues. While standard surgical planning uses radiology to obtain cross-sectional or volumetric images of the location of solid tumors preoperatively, surgeons rely mostly on palpation and visual inspection of the tissue during the actual procedure to distinguish malignant lesions from healthy tissue [1–5], with intraoperative image guidance still the exception due to its complex setup [6]. This limited technique could result in failure to surgically resect all positive surgical margins (PSM), which are associated with a higher risk of recurrence, poor prognosis, and necessary adjuvant treatments—radiotherapy, hormone therapy, chemotherapy, or repeat operations [1, 2]. Generally, techniques to assist surgeons

✉ Jan Grimm
grimmj@mskcc.org

1 Department of Chemistry and Biochemistry, The City College of New York, 160 Convent Avenue, New York, NY 10031, USA

2 Ph.D. Program in Chemistry, The Graduate Center of the City University of New York, New York, NY 10016, USA

3 Molecular Pharmacology Program, Memorial Sloan Kettering Cancer Center, New York, NY 10065, USA

4 Department of Radiology, Memorial Sloan Kettering Cancer Center, New York, NY 10065, USA

5 Pharmacology Program, Weill Cornell Medical College, New York, NY 10021, USA

6 Department of Radiology, Weill Cornell Medical College, New York, NY 10021, USA

in the identification of resection margins have included the clinical use of histology and cytology techniques during surgery [1]. A gold-standard being intraoperative frozen section-analysis (IFS), a real-time histopathological technique that is both labor-intensive and resource-consuming, is limited in sensitivity and specificity [2, 7]. A form of IFS used for radical prostatectomy, neurovascular structure-adjacent frozen-section analysis (neuroSAFE), shows more accurate IMA [7], but can only survey samples from the posterolateral part of the prostate [4] and reports high false negative rates [8, 9]. Patients undergoing surgical resection can suffer from inadequate complete removal of the tumor because the current modalities are not sufficiently reliable.

This clinical need has motivated the development of novel imaging techniques for IMA in surgical oncology. One systematic review identified 16 different categories of IMA techniques: fluorescence, advanced microscopy, ultrasound, radiography, optical coherence tomography (OCT), MRI, elastic scattering spectroscopy (ESS), bioimpedance, CT, mass spectrometry, Raman spectroscopy, nuclear medicine imaging, terahertz imaging, photoacoustic imaging, hyperspectral imaging, and pH measurement [6]. Radiography and ultrasound are some of the more feasible techniques for use in breast cancer and prostate cancer [10]; however, the diagnostic accuracy was found to be quite low for both modalities [6]. A case study was published for one patient with prostate cancer (PCa) and four patients with biochemical recurrence using ^{111}In-PSMA-I&T inhibitor for radio-guided surgery [10]. A gamma probe in combination with an optical tracking system (declipseSPECT) was able to reconfigure a 3D image overlaid with a live video stream of the surgical field [10]. A randomized study on 134 patients with palpable T1–T2 invasive breast cancer determined that ultrasound-guided surgery using a 15-MHz probe could reduce rates of PSM, all while reducing the amount of healthy tissue removed [11]. Similarly, while ultrasonography is compact, portable, and less expensive, the contrast can be quite low due to high speckle [3]. Other radiological modalities including CT, OCT, and MRI for IMA generate cross-sectional anatomical images and do not necessarily require the use of contrast agents [6]. OCT, with a penetration depth of ~ 2 mm and spatial resolution near cellular level (~ 10 uM), can be produced using a handheld device with a detection comparable to histology [6]. Intraoperative use of CT and MRI is limited by equipment configuration (i.e., magnetic field, surgical site accessibility) prior to seamless translation into the clinic, although, a resolution close to 1 mm is ideal. MRI is superior in soft tissue contrast but requires long acquisition times. A randomized controlled study was performed using 58 glioma patients to determine whether intraoperative MRI assists surgeons in performing a complete resection during neurosurgery [12]. Even with the addition of a large magnet in the surgical suite and increased time for imaging acquisition, the radiographic total resection was 98% using MRI-guided surgery compared to the 68% achieved with only the surgeon's expertise [2, 12].

A few optical IMA modalities worth highlighting are elastic scattering spectroscopy (ESS) and Raman spectroscopy, which characterizes margins based on the interaction between light and tissue [6]. A study was concluded on the use of Raman spectroscopy to assist surgeons in the resection of breast tissue from six patients receiving a mastectomy [13]. This was done using the new generation of Raman spectrometers that are commercially available, portable, and affordable [13]. Another study showed that ESS was able to image sentinel lymph nodes for breast cancer metastases and determination of surgical resection type [14]. With a sensitivity of 85% and a specificity of 94%, a prospective clinical trial would be a necessary next step towards clinical adaption for this modality [14]. While these techniques may demonstrate difficult clinical integration, slow acquisition times, and the inability to sample the entire margin, they show the field of IMA is ever evolving [6]. Similarly, the use of mass spectrometry to characterize aerosols released during electrosurgery is a near real-time innovative approach to IMA [6]. The challenges of adapting mass spectrometry into clinical setting includes the cost of instrumentation and the time required to develop the MS-based medical device and a spectral database [15]. All the above mentioned techniques are hindered by limitations in sensitivity, specificity, tissue penetration, accuracy, cost, and real-time detection.

The most common modality for IMA is, by far, fluorescence, which has been demonstrated, amongst others, in breast cancer, liver metastases, and bypass graft surgery [5]. Fluorescence provides real-time feedback to surgeons with limited penetration depth (< 10 mm) [6]. In the application of intraoperative fluorescence, the detection of deep-seated tumors is less important; in fact, the limited penetration depth allows for the signal of only surface tumor cells to be imaged, allowing for surgeons to diagnose surgical margins (~ 5 mm). The penetration depth can also be optimized based on wavelength excitation and emission. ICG is one of the most commonly used FDA-approved fluorescent agents that emits in the NIR region; however, it is non-specific towards cancer types, leading to a low tumor-to-background ratio [5]. Targeting moieties can greatly improve accuracy for this modality; however, these agents must undergo extensive FDA regulations to gain access to clinical setting [6]. This has slowed large multicenter clinical studies from evaluating the efficacy of fluorescence imaging systems for diagnostic or intraoperative ability [5]. Nonetheless, there are countless clinical trials on novel targeted fluorescent tracers. One of the most recent agents to reach phase 3 clinical trials is bevacizumab-IRDye800CW, which targets the vascular endothelial growth factor (VEGF) in breast cancer patients (NCT05939310). This modality can intraoperatively

image the ex vivo specimen and the surgical cavity using a multispectral fluorescence reflectance imaging (MFRI) camera. Recent results published from a phase 2a clinical trial evaluated the feasibility of prostate-specific membrane antigen (PSMA) fluorescent tracer OTL78 for targeted real-time imaging during robot-assisted radical prostatectomy [16]. A near-infrared (NIR) dye S0456 conjugated to the glycoprotein through a PEG linker was used for in vivo and ex vivo intraoperative imaging of prostate cancer patients [16]. Results published from a phase 1 clinical trial assessed IS-0002, a NIR fluorescently labeled PSMA-targeting peptide, as an ex vivo and in vivo intraoperative imaging agent for prostate cancer patients [17]. Normal tissue was differentiated from tumor tissue at all doses, except at high doses the background signal was too high, which led to false positives and reduced diagnostic accuracy [17].

CLI is a relatively new optical modality that utilizes the blue Cerenkov light emitted by particle emissions from radioisotope decay. CLI should not be overlooked when addressing modalities for IMA. This review recognizes that CLI has within its framework the potential to bridge the gap between targeted fluorescent agents and clinically used radiotracers, for use in intraoperative imaging [18]. CL is a promising technique that allows real-time visualization of molecular events and enables the use of widespread optical imaging equipment to visualize clinical diagnostic and therapeutic radionuclides. As a result, CLI is a promising molecular imaging technique for analyzing resection margins, mostly in a back-table setting (i.e., of the resected specimen and not the patient cavity). The autofluorescence of the specimen is eliminated, as no excitation source is required, resulting in higher signal-to-background ratios albeit at lower signal intensities. It also allows for the imaging of multiple subjects concurrently, providing cost and time benefits [19]. CLI is particularly interesting for image-guided cancer surgery, as it allows the use of clinically approved tumor-targeted PET tracers and small sized imaging equipment fit for clinical setting [1]. As demonstrated later, CLI enables surgeons to accurately identify tumor margins and detect metastatic lesions. This non-invasive imaging modality has the potential to revolutionize surgical procedures by improving precision and reducing the need for multiple surgeries.

Cerenkov luminescence technology for molecular imaging

Cerenkov radiation was systematically characterized by Pavel Cerenkov in 1934, in collaboration with Ilja Mikhailovic Frank and Igor Yevgenyevich Tamm, which led to their Nobel Prize in Physics in 1958[1, 19–23]. Figure 1 illustrates the Cerenkov phenomenon, wherein a charged subatomic particle (positron/electron) travels faster than the velocity of light specific to the dielectric medium the particle is traveling through—i.e., a supra-relativistic subatomic charged particle [19–23]. Bipolar molecules like water align themselves along the path of the charged particle causing asymmetrical polarization and a dipole electric field [19–23]. As the charged particle moves through the medium, the polarized molecules return to their ground state, releasing energy as photons, which can be detected using an electron-multiplying charge-coupled device (EMCCD) camera in a light-sealed space [19–23]. CL is entirely dependent on the interaction between the charged particle and the medium it traverses [21]. The production of CL is lost once the charged particle loses enough kinetic energy to its surroundings and travels below the Cerenkov threshold [19–23]. This threshold is dependent on the phase velocity of the medium, which correlates to the refractive index of the medium (n). For instance, water ($n = 1.33$) has a Cerenkov threshold of 0.264 MeV, whereas tissue ($n = \sim 1.4$) has a threshold of 0.219 MeV, so the number of CL photons emitted from tracers will be somewhat larger in tissue than in water [21]. CL emits wavelengths ranging from ultra-violet to short-wave infrared (350–1300 nm), with a peak in the UV and blue-weighted region [1, 24]. The shorter wavelengths are heavily attenuated in biological tissue, limiting CL to penetrate only superficial layers of tissue in the visible spectrum, but can go deeper if detecting longer wavelengths [1, 24]. The emission properties of CL positions it well as a modality for superficial molecular imaging of excised specimens for cancerous lesions labeled with a radiotracer.

Molecular imaging methods generally have higher sensitivity and specificity than conventional imaging. It is most often used for detection of lymph node metastases [9]. CLI has the advantage of combining the availability, sensitivity, and specificity of nuclear tracers for molecular imaging with the higher resolution and faster acquisition times of optical imaging [1]. For example, CLI has the capacity to image the entire surface of the prostate at once compared to IFS analysis, which is done in slices [1, 9]. Compared to other molecular imaging modalities such as PET or SPECT, CLI would offer lower costs, faster acquisition times, real-time detection, and compact imaging equipment [1, 25]. The most salient advantage of CLI is, by far, the ability to use FDA-approved PET tracers to produce CL, which allows for both optical and nuclear molecular imaging [1, 25]. In fact, PET imaging measures the annihilation of emitted positrons by electrons, whereas CLI measures the Cerenkov photons produced from the emitted positrons [1]. This commonality would allow for bimodal imaging (optical /PET) of a patient's condition using a single radiotracer. However, the low signal is a drawback of CL for in vivo imaging due to high

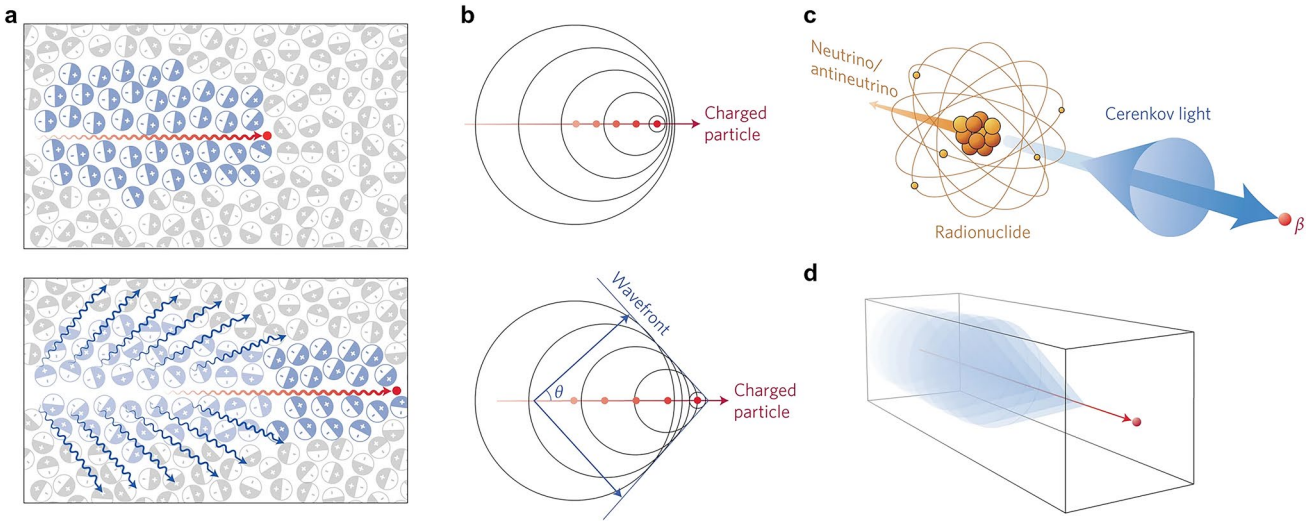

Fig. 1 Cerenkov luminescence phenomenon. **a** Top: Charged particle (red line) traveling faster than the velocity of light in a particular dielectric medium, i.e. water or tissue, asymmetrically polarizing the medium to create a dipole electric field. Bottom: As particle moves through medium, the molecules return to ground state, emitting blue-weighted light in the forward direction (blue lines). **b** A photonic wavefront is formed from constructive interference of the coherent waves produced in a forward angle θ. **c** Radionuclides that emit β-particles in a dielectric medium with energies greater than the Cerenkov threshold produce CL. **d** A medium with a negative refractive index shows the CL cone is pointing in the reverse direction. Reproduced with permission from [20], © 2017 Springer Nature Limited

attenuation. A latent solution would be the integration of SWIR imaging to enhance CL signal and eliminate the need for a dark enclosure. Currently, SWIR systems are still in preclinical phase, so there is more work needed before these can be implemented to compare to other modes of in vivo image-guided surgery.

CLI has rapidly gained interest in the molecular imaging field and has been proposed for various applications in scientific research [22]. Efforts have been made to transform CLI into a tomographic technique and to shift the Cerenkov emission into a more suitable range for biological applications [22]. The very first application of Cerenkov-producing PET radiotracers in vivo was in 2009 by Robertson et al. which led to the adoption of this technology in the field of biomedical imaging [26]. Holland et al. first demonstrated the preclinical use of CLI for intraoperative surgical resection of tumors in 2011 [27]. Figure 2 depicts the first Cerenkov image from a human patient, using ^{131}I for hyperthyroidism; another study in the same year used CLI to image nodal disease using ^{18}F-FDG [28, 29]. More recently, Pratt et al. reported in 2022 the largest study to date using CLI to image tumor lesions in 96 patients with various types of tumors and radiotracers, including therapeutic agents [30]. In this first large-scale human clinical trial, CLI could localize lymphoma, thyroid, pancreatic, and neuroendocrine tumors, and simultaneously monitor tumor therapy (NCT01664936). The following section of this review will provide all relevant clinical applications of CLI for IMA.

Applications of CLI for intraoperative margin assessment

A 2015 clinical study demonstrated the first use of endoscopic CLI (ECLI) for detection of gastrointestinal disease using an EMCCD camera attached to a flexible fiber endoscope [31]. Four patients prescribed ^{18}F-FDG injection for diagnosis and metastatic detection were selected for whole-body PET, followed by ECLI in a dark room [31]. Using a 5-min exposure time, the study proved that there was a linear relationship between ECLI measurements, and the activity measured using PET [31]. The environment of the colon is an anatomical dark chamber well suited for the use of CLI to detect colon tumors within the superficial layers of the lumen [1, 31]. This technique would also be applicable to other forms of endoscopy including upper GI endoscopy, bronchoscopy, hysteroscopy, and laparoscopy for simultaneous morphological and functional imaging [1, 31]. Another early study from 2016 completed the first imaging of a single patient's meningioma labeled with ^{90}Y-DOTATOC using peptide receptor radionuclide therapy (PRRT)[32]. An imaging device made in the lab was used to analyze the excised brain tumor using a 5-min exposure time. CLI was compared to radio-luminescence imaging (RLI) using a plastic scintillator that maximizes the light detected. The localization of the CLI and RLI radiance aligned with the tumor region, but it was determined that RLI had increased background noise outside of the sample region. Therefore, the study concluded

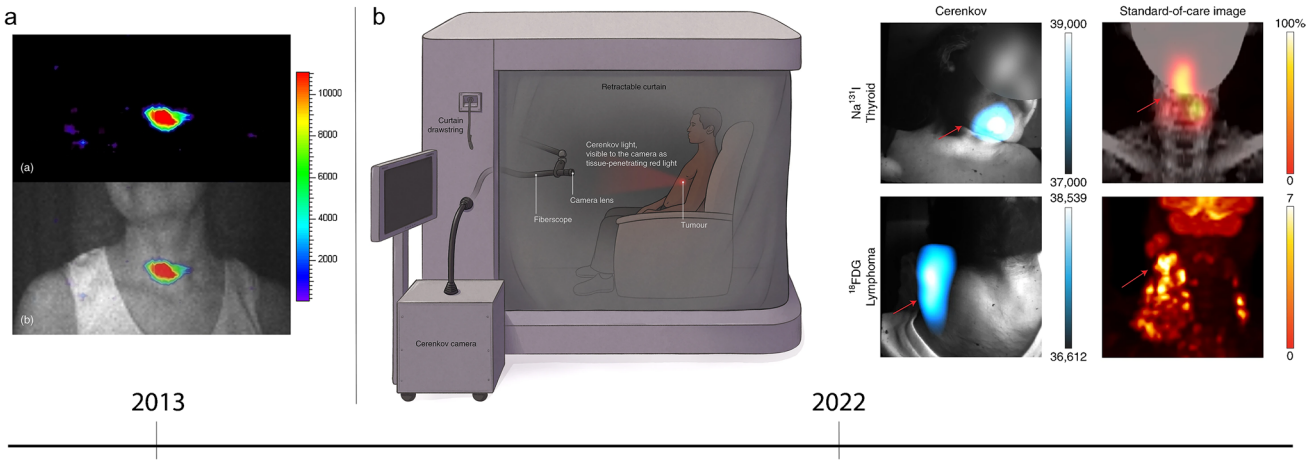

Fig. 2 Clinical Cerenkov fiberscope imaging of cancer patients. **a** (top) Early CLI of a patient's thyroid. (bottom) CL and gray scale overlay confirms CL is coming from the thyroid gland. Reproduced with permission from [28], © 2013 SPIE. **b** (left) After radiotracer injection, the patient sits in the lightproof enclosure for up to 15 min of imaging time. The Cerenkov camera is placed outside the enclosure and connected to relay optics, fiberscope, and a f-0.95 lens. Most of the CL detected is red-weighted, since the blue-weighted wavelengths are attenuated and scattered through the patients' tissue. (right) CL image produced using the clinical Cerenkov setup vs. a standard-of-care PET image of (top) thyroid cancer using [^{131}I]-sodium iodide and (bottom) lymphoma using [^{18}F]-FDG. Reproduced with permission from [30], © 2022 Springer Nature Limited

that CLI would be a more specific modality for imaging excised tumors [32].

The first clinical study on the feasibility of ^{18}F-FDG CLI for intraoperative detection of tumor margins in breast conserving surgery (BCS) using wide local excision (WLE) was performed in 2017 using the LightPath®, a then commercial device from LightPoint Medical as shown in Fig. 3 [33, 34]. Imaging settings were optimized in the first ten patients, and the remaining 12 patients were included in the dataset [33]. It was found that an acquisition time of 300 s provided optimal imaging settings with a resolution of 1.25 mm [33]. Ten out of the 12 patients had an elevated tumor radiance ($t^{1/2} = 115.5$ min) that correlated to the half-life of Fluorine-18 ($t^{1/2} = 109.8$ min) [33]. Interestingly, the

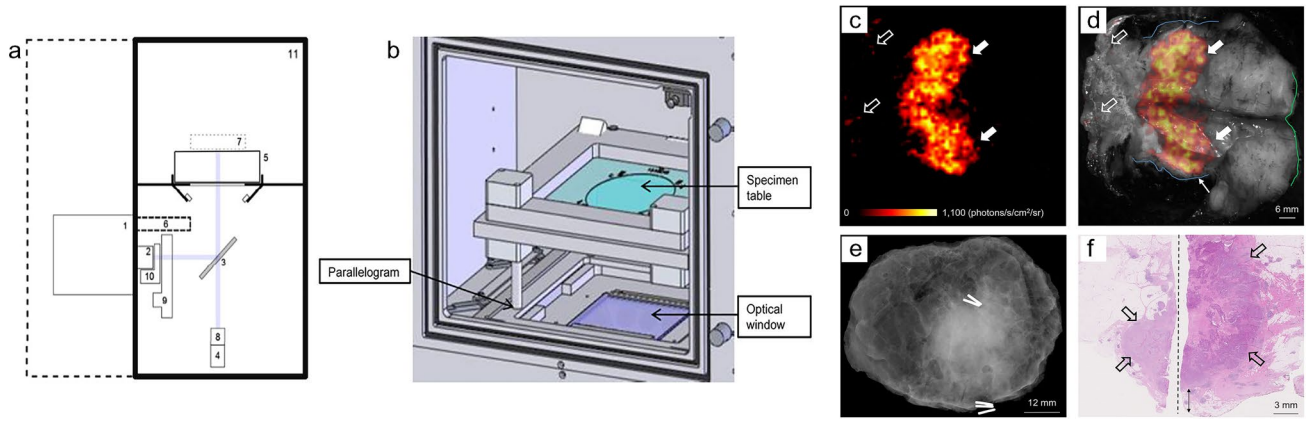

Fig. 3 Investigational intraoperative CLI imaging of WLE specimen. **a** Schematic diagram of Lightpath® (Lightpoint Medical Ltd. UK) imaging system: (1) EMCCD camera, (2) f-0.95 lens, (3) Hinged reflex mirror, (4) complementary metal oxide semiconductor reference camera, (5) specimen table, (6) lead radiation shielding for EMCCD camera, (7) focal zone, (8) fixed lens for reference camera, (9) filter wheel, (10) LED RGB light array, (11) specimen chamber. **b** Specimen chamber: Table can be positioned using a parallelogram to center specimen within the optical window. **c** Cerenkov image of WLE specimen from patient with grade 3, estrogen receptor-negative/human epidermal growth factor receptor 2-negative, NST carcinoma, mean radiance of 871 ± 131 photons/s/cm^2/sr and mean TBR is 3.22 (white arrows); phosphorescent signal was detected from pathology ink (open arrows). **d** Gray-scale image overlaid with Cerenkov image; both surgeons measured the posterior margin to be 2 mm (blue outline). **e** Specimen radiography image. **f** Histopathology image of primary tumor confirmed to have a posterior margin of 3 mm (double arrow). This research was originally published in J Nuclear Med. [33] Grootendorst, M. R. et al. J Nucl Med. 2017;58(6):891–898. © 2017 SNMMI

two patients with no tumor radiance had significantly lower levels of activity detected along with a smaller tumor size [33]. However, the only two cases of PSM confirmed by histopathology were not able to be measured by CLI because the lesion was in the medial margin [33]. While it was concluded that CLI would be a promising, low-risk option for intraoperative molecular imaging, suppressing image artifacts (described below) from the diathermy-induced chemiluminescence was only later addressed by Darr et al.[9, 33].

In recent years, CLI has most prominently been used for intraoperative molecular imaging in a backtable approach (i.e., imaging ex vivo specimen) of primary prostate cancer (PC) using ^{68}Ga-PSMA, ^{18}F-PSMA, and ^{18}F-choline PET tracers [4, 8, 9, 35–37]. The first-in-human feasibility study for ^{68}Ga-PSMA intraoperative CLI assessment of surgical margins was reported in 2015 and 2020; the workflow is described in Fig. 4 [4, 8, 38]. Compared to histopathological analysis of excised prostate specimen, both studies showed that CLI could be used to differentiate between PSM and NSM in at least 60% of the patients [4, 8]. Imaging was completed with 150–300 s exposure times and 8 × 8-pixel binning in approximately 20 min [4, 8]. The commonality of false-positive signals near the prostate base and bladder neck was reasoned to occur because of the renal clearance of Gallium-68 [4, 8, 9]. So, to avoid contamination, the prostate glands were either rinsed (1–2 ×) in sodium chloride solution or drained using a catheter before surgery commenced [4, 8, 9, 35–37]. However, Heuvel et al. did a study on the background signal of excised prostate due to electrosurgery (diathermy) commonly used at the prostate base, which raises the intracellular temperature, producing a (potential chemiluminescence) signal (400–710 nm) that overlaps with the emission of CL (350–1000 nm). The chemiluminescence was consistently observed in nonradioactive specimens, confirming that this signal was independent of the tracer injection, especially as the intensity did not reduce in over an hour (^{68}Ga $t^{1/2}$ = 68 min) [36]. In multiple studies, a 550-nm optical short pass filter (OF) was used to test whether false-positive signals were a result of the longer CL wavelengths traveling to the surface from within the prostate gland [4, 9, 36]. Darr et al. further studied the use of a 550-nm OF to retrieve higher specificity from filtering out the more penetrating CLI wavelengths when analyzing resection margins [4, 9]. It was determined that the high false-positive rates near the prostate base due to diathermy could be virtually eradicated using the 550-nm OF [4, 9]. This filtering is most likely successful because it has been determined that any CL leaving the body is above 600 nm due to hemoglobin absorption, so any signal below is not attributable to CL [30]. Another method used to reduce background signal is flexible autoradiography (FAR), which successfully enhanced the tumor-to-background ratio (TBR) 2.1–3.2 times by increasing light output from beta-emitting isotopes [36, 37]. This consists of using a flexible ultra-thin scintillator film, but because the film is opaque, it is hard to discern the anatomical and spatial information by overlaying both images [36, 37].

Current clinical trials are in progress at King's College London, to study the diagnostic accuracy of intraoperative CLI + FAR using the LightPath® imaging system for

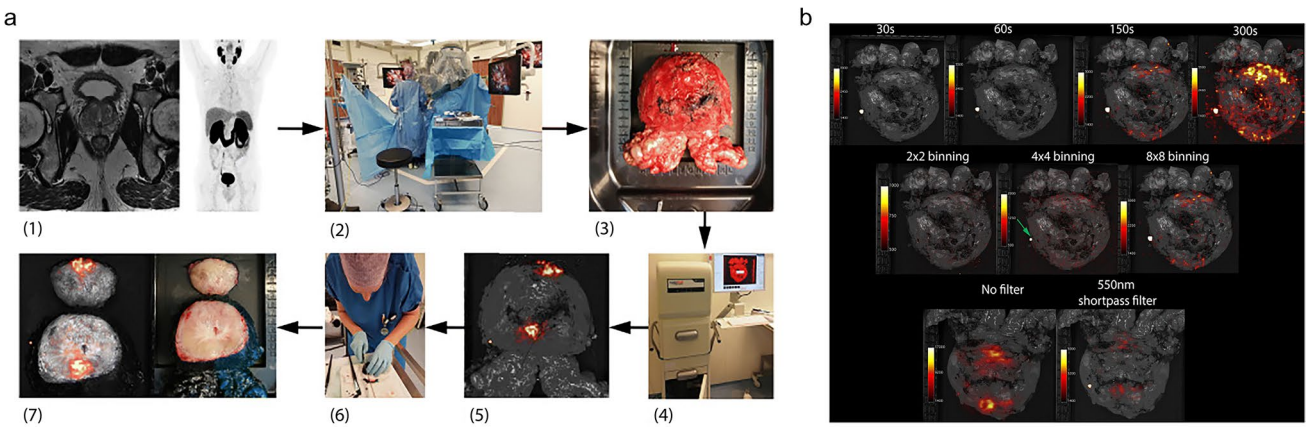

Fig. 4 Workflow and settings used for intraoperative CLI of prostate tumor. **a** (1) Preoperative ^{68}Ga-PSMA PET-CT and MRI scan. (2) ^{68}Ga-PSMA is administered via i.v. injection during surgery. Once prostate is removed using the da Vinci® surgical system, the specimen is rinsed with NaCl solution. (3) Prostate is placed on specimen table (4) Lightpath® images all six sides. (5) Unfiltered Cerenkov image produced. (6) Specimen is inked and cleaved ~ 1 cm from the apex. (7) White-light (right) and Cerenkov (left) image of cleaved prostate. **b** Top row: 8 × 8 binning and 550 nm filter used for images of varying exposures of 30 s (TBR 1.10), 60 s (TBR 1.18), 150 s (TBR 1.85), and 300 s (TBR 1.98). Center row: 150 s exposure and 550 nm filter used for images of varying pixel binning of 2 × 2 (TBR 1.06), 4 × 4 (TBR 1.26), 8 × 8 (TBR 1.85). Bottom row: 150 s exposure and 8 × 8 binning used for images without filter and with 550 nm filter. This research was originally published in Eur. J. Nucl. Med. Mol. Imaging. [4] Olde Heuvel, J. et al. EJNMMI. 2020;47(11):2624–2632. © 2020 Springer Science + Business Media

breast tumor margin assessment (NCT05496101). Lightpoint Medical Limited (recently acquired by Telix Pharmaceuticals) has conducted another clinical trial on correlating resection margin status of breast cancer tumors and metastatic status of axillary lymph nodes using proprietary EnLight® and Lightpath® imaging systems compared to histopathology analysis (NCT02151071). Xijing Hospital of Digestive Diseases is testing multimodal ECLI to obtain structural and functional imaging of early-stage rectal cancer (NCT05575765). Clinical results have not been published yet, but the effect of MF fiber diameters, fiber material, and probe coating on ECLI efficiency has been evaluated to inform a second generation ECLI device, however, extensive biosafety assessment and preclinical validation is required to reach the clinic [39]. Finally, we are preparing to conduct a further clinical trial at Memorial Sloan Kettering Cancer Center to test an improved version of the clinical CLI system depicted in Fig. 2 (NCT03484884).

Further developments in CLI for intraoperative margin assessment

Overall, the intraoperative CLI protocols across cancer types were similar in terms of exposure times and pixel binning. Olde Heuvel et al. explored the effect of exposure time (30–300 s) on the tumor-to-background ratio (TBR) and described an increase in TBR values as the exposure time increased as seen in Fig. 4b [4]. This study also showed the effect of pixel binning (2×2 vs. 4×4 vs. 8×8) on TBR and showed an increasing trend in TBR values as the pixel binning was increased [4]. It is important to note that while certain exposure times and pixel binning were deemed most optimal for studies on intraoperative CLI, these settings will require optimization based on the radioisotope and dose injected. Two studies explored the effect of a 550-nm optical short pass filter and recorded a significant reduction in TBR values, which corresponded to false positive signals from electrosurgical diathermy [4, 9]. All clinical studies testing CLI for radical prostatectomy considered the renal clearance of radioisotopes, such as ^{68}Ga-PSMA-11, and drained the prostate prior to surgery using a catheter [8, 9, 37]. In addition, the resected specimen was most often rinsed or wiped down at least once with a saline solution to remove any signal coming from residual urine [8, 9, 37]. The largest variation was seen in the imaging apparatus dependent on whether the CLI was used to image ex vivo specimen or an anatomical dark chamber such as the colon [31]. This shows the versatility of CLI, which requires an EMCCD camera and a light-tight imaging chamber, as this set-up is also compatible with flexible fiber endoscopes for various applications in upper GI endoscopy, bronchoscopy, hysteroscopy, and laparoscopy [1, 31].

To determine whether CLI is feasible for intraoperative tumor evaluation, the safety of medical staff in terms of radiation exposure is crucial, particularly because PET tracers have higher energy and generate more annihilation γ-photons [40]. To verify the CLI intraoperative surgical margin evaluation, Costa et al. quantified the occupational radiation exposure during CLI-assisted robot-guided radical prostatectomy (RP) and the histology required. In this trial, ten patients with preoperative PET/CT-determined high-risk or intermediate prostate cancer received a single ^{68}Ga-PSMA-11 injection at a dose of about 141.9 ± 57.86 MBq [40]. The patient's dosage rate was determined at four locations of interest, 1 m away from the patient, to correspond with the positions of the medical staff: [A] head, [B] right side, [C] left side, and [D] feet. Using a germanium detector rather than a ring dosimeter, the level of activity in the prostate specimen was used to calculate the exposure of the histology personnel. The average activity was 2.96 kBq, which was less than the permitted limit of 100 kBq for gallium-68 [40]. The following staff exposure levels were measured using electronic personal dosimetry (EPD): scrub nurse (3.3 ± 3.9 µSv), CLI imager/surgeon (0.7 ± 0.7 µSv), and first surgical assistant (9.0 ± 7.1 µSv) [40]. However, below the 1–9.99 µSv range found for ^{99m}Tc sentinel lymph node operations, the EPD estimations are imprecise. If fewer than 110 ^{68}Ga-PSMA-11 intraoperative CLI procedures were performed annually, the first surgical assistant would be exposed to tolerable levels of occupational risk during a single injection [40]. The creation of an anthropomorphic mathematical phantom that can overcome the drawbacks of point-source calculations and more faithfully depict the source is a task for future research [40]. Furthermore, in terms of radiation exposure, based on this study, other longer-lived radionuclides, such as ^{64}Cu and ^{89}Zr, could be appropriate for intraoperative CLI tumor assessment. Grootendorst et al. reported the radiation exposure for personnel using electronic personal radiation dose monitors during intraoperative ^{18}F-FDG CLI assessment of tumor margins in breast conserving surgery. In 2015, the results of the first eight patients were published and the average dose per procedure (µSv) is as follows: surgeon (28.6), anesthetist (8.6), anesthetist assistant (6.4), scrub nurse (1.8), and recovery nurse (6.6) [34]. In 2017, the list of medical staff and number of patients were expanded and the average dose per procedure (µSv) was as follows: surgeon (34), anesthetist (11), nuclear medicine technologist (9), anesthetist assistant (6), trial coordinator (21), recovery nurse (4), scrub nurse (2), periphery nurse (1), research fellow (1), ward nurse (0), and tissue biobank practitioner (0) [33]. It is important to note that the levels of radiation are increased, especially for the surgeon, because the surgery is not a robot-assisted procedure. In 2015, Michel et al. published early results of the PRIME (PRostate Imaging for Margin Evaluation) study using ^{18}F-choline to assess margin status

using intraoperative CLI in three prostate cancer patients. The average radiation dose (μSv) was measured using badge dosimeters as follows: assisting surgeon (145), scrub nurse (60), anesthetic staff (< 20), and all other staff (< 10)[35]. These exposure levels were quite high considering the radical prostatectomy was performed using robot-assisted technology, which shows the need for a consistent, methodical way to measure radiation exposure during these procedures.

Olde Heuvel et al. used clinically relevant activity levels in vitro, ascertained by ^{68}Ga-PSMA PET/CT in 30 patients, to examine the efficacy of ^{18}F against ^{68}Ga for CLI intraoperative margin evaluation [41]. Because ^{18}F has a lower positron energy than ^{68}Ga, it was assumed that ^{68}Ga would provide a greater signal-to-noise ratio (SNR). Compared to the conventional settings used for ^{18}F (300 s exposure, 8 × 8 binning), the optimum settings for ^{68}Ga CLI was 120 s exposure and 2 × 2 binning, which shortened the acquisition duration for clinical use [41]. By increasing either the exposure time or pixel binning, the SNR increases and the radiation dosage can be lowered, providing higher contrast, and reduced occupational exposure. It was found that in comparison to ^{18}F, ^{68}Ga generated CL light production 22 times higher [41]. Additionally, the limit of detection for ^{68}Ga was significantly lower at 1.2 kBq/mL than that of ^{18}F, which was 23.7 kBq/mL [41]. Because of the larger positron range, the spatial resolution was somewhat poorer for ^{68}Ga; nevertheless, as surgeons cannot perform resection with micrometer efficiency, this would not impede clinically important demands [41]. It was proposed that filters may be employed only to look at CLI on the surface of prostate specimens; the depth of the CLI signal was not assessed in this investigation [41]. More work is needed to determine the efficacy of various other isotopes; however, ^{18}F and ^{68}Ga are the most relevant when considering FDA-approved PET tracers.

In more recent years, there has been an expanding number of approved PSMA-targeted PET tracers for prostate cancer. Before this, ^{18}F-FACBC, or ^{18}F-fluciclovine, an amino acid analog, was used to target malignancies with upregulated amino acid transport [42]. While this tracer was not specific to prostate cancer, it did provide high sensitivity, specificity, and accuracy for the staging and follow-up postprostatectomy for radiation therapy planning, which reduces biochemical recurrence [42]. PSMA tracers have largely replaced ^{18}F-fluciclovine since its FDA-approval in 2016; however, there are some advantages to this tracer that relate to CLI for IMA [42]. For instance, there is minimal activity found in the excreted urine of patients and could be helpful in the 10% of prostate cancers that are PSMA-negative [42]. In 2020, ^{68}Ga-PSMA was FDA-approved for PET scans using the targeted transmembrane protein, PSMA, overexpressed in prostate cancer, which was only available from two manufacturers (UCLA and UCSF) [42]. In 2021, the FDA approved a kit to produce ^{68}Ga-PSMA-11, or ^{68}Ga-gozetotide, making it more accessible to patients [42]. Around the same time in 2021, ^{18}F-DCFPyL, or ^{18}F-piflufolastat, was the first ^{18}F PSMA PET tracer that could potentially improve spatial resolution, quantitation, and tumor-to-background ratio, allowing for better detection of lower-grade or smaller sized prostate cancers [42]. This PET tracer also had better stability, creating a larger production capacity. Just recently in 2023, the FDA approved ^{18}F-rhPSMA-7.3, or ^{18}F-flotufolastat, with an optimized affinity, leading to higher specificity in prostate cancers with low PSA levels [43]. Overall, PSMA PET scans are deemed to be more accurate than CT or bone scans, and older non-specific PET tracers, including ^{11}C-choline and ^{18}F-fluciclovine, and is effective at imaging lesions in the prostate, lymph nodes, soft tissue, and bone [42]. The PSMA tracers are renally excreted and accumulate in the bladder, which explains the necessity of draining the bladder before intraoperative CLI of the prostate specimen. CLI using ^{68}Ga-PSMA has shown promising results in detecting positive surgical margins and visualizing prostate cancer tissue at the resection margin [4, 8, 41]. The technique has demonstrated the ability to distinguish between positive and negative surgical margins and has the potential to reduce the number of positive surgical margins during radical prostatectomy.

Conclusion

Overall, these studies show that CLI is a feasible clinical modality, yet still in its infancy. A quantitative approach needs to be further optimized as the attenuation and scattering of CLI in tissue are likely to vary across patients [4]. The spatial accuracy is far greater using histopathological analysis and a microscope than macroscopic to mesoscopic CLI at a resolution of 1–2 mm; however, using an isotope with lower positron energy would provide better resolution and pixel binning, and exposure times can be optimized to still achieve high TBR values [41]. More work needs to be done on depth analysis of CLI to allow for a standardized method to detect tumor margins within 5 mm from the surface of the specimen [4]. Since CLI relies on radiotracers, further exploration to detect deeper lesions can be proceeded first with handheld radiodetectors and then with CLI. A dose calibrator should be used to estimate activity in real-time to correlate with CLI instead of using PET measurements from earlier in the procedure, although they should provide reasonable information as well and is more suitable in a clinical context [4]. Effects of electrothermy on CLI need to be further explored and managed through filtering, which has been used successfully [4, 9, 36]. The benefits of CLI are the relatively low radiation exposure, rapid acquisition, and the ability to seamlessly layer anatomical and optical images [1, 4]. Concern of exposure to patient and personnel

has been so far minimal if in the hands of experienced teams that perform radio-guided surgeries (i.e., in dedicated centers), but more work needs to be done to quantify these exposure levels consistently. The recent discovery that CL can be detected in the short-wave infrared region (SWIR) can eliminate the need for a dark enclosure with the use of non-SWIR emitting LEDs, which would revolutionize the clinical feasibility of CLI and allow surgeons to image in a well-lit room using LEDs without a SWIR component [24]. Right now, CLI could be used to guide a more detailed histopathological evaluation in combination with established methods such as neuroSAFE [4]. However, there is a need for larger scale studies with a standard operating protocol before this modality reaches widescale use [9].

Author contribution Jan Grimm conceptualized the idea for the article and approved final manuscript. Natalie Boykoff performed the literature review, data analysis, and drafted the manuscript.

Funding N.B. is grateful for support from the Sol & Bettina Kornbluh Fund, and for Fellowship support from IDEALS II, NSF #2112550. We acknowledge the support of the following grant: P30 CA08748 (to S. M. Vickers MSKCC).

Data Availability Data sharing is not applicable to this article as no new data were created or analyzed in this study.

Declarations

Competing interests The authors declare no competing interests.

References

1. Grootendorst MR, et al. Cerenkov luminescence imaging (CLI) for image-guided cancer surgery. Clin Transl Imaging. 2016;4(5):353–66.
2. Rosenthal EL, et al. The status of contemporary image-guided modalities in oncologic surgery. Ann Surg. 2015;261(1):46–55.
3. Wilson BC, Eu D. Optical spectroscopy and imaging in surgical management of cancer patients. Translational Biophotonics. 2022;4(3):e202100009.
4. Olde Heuvel J, et al. 68Ga-PSMA Cerenkov luminescence imaging in primary prostate cancer: first-in-man series. Eur J Nucl Med Mol Imaging. 2020;47(11):2624–32.
5. Chi C, et al. Intraoperative imaging-guided cancer surgery: from current fluorescence molecular imaging methods to future multi-modality imaging technology. Theranostics. 2014;4(11):1072–84.
6. Heidkamp J, et al. Novel imaging techniques for intraoperative margin assessment in surgical oncology: a systematic review. Int J Cancer. 2021;149(3):635–45.
7. Schlomm T, et al. Neurovascular structure-adjacent frozen-section examination (NeuroSAFE) increases nerve-sparing frequency and reduces positive surgical margins in open and robot-assisted laparoscopic radical prostatectomy: experience after 11,069 consecutive patients. Eur Urol. 2012;62(2):333–40.
8. Darr C, et al. Intraoperative ⁶⁸Ga-PSMA Cerenkov luminescence imaging for surgical margins in radical prostatectomy: a feasibility study. J Nucl Med. 2020;61(10):1500–6.
9. Darr C, et al. Prostate specific membrane antigen-radio guided surgery using Cerenkov luminescence imaging—utilization of a short-pass filter to reduce technical pitfalls. Transl Androl Urol. 2021;10(10):3972–85.
10. Maurer T, et al. Prostate-specific membrane antigen-radioguided surgery for metastatic lymph nodes in prostate cancer. Eur Urol. 2015;68(3):530–4.
11. Krekel NM, et al. Intraoperative ultrasound guidance for palpable breast cancer excision (COBALT trial): a multicentre, randomised controlled trial. Lancet Oncol. 2013;14(1):48–54.
12. Senft C, et al. Intraoperative MRI guidance and extent of resection in glioma surgery: a randomised, controlled trial. Lancet Oncol. 2011;12(11):997–1003.
13. Zúñiga WC, et al. Raman spectroscopy for rapid evaluation of surgical margins during breast cancer lumpectomy. Sci Rep. 2019;9:14639. https://doi.org/10.1038/s41598-019-51112-0.
14. Zhu Y, Fearn T, Chicken DW, et al. Elastic scattering spectroscopy for early detection of breast cancer: partially supervised Bayesian image classification of scanned sentinel lymph nodes. J Biomed Optics. 2018;23(08):085004.
15. Balog J, et al. Intraoperative tissue identification using rapid evaporative ionization mass spectrometry. Sci Transl Med. 2013;5(194):194ra93–194ra93.
16. Stibbe JA, et al. First-in-patient study of OTL78 for intraoperative fluorescence imaging of prostate-specific membrane antigen-positive prostate cancer: a single-arm, phase 2a, feasibility trial. Lancet Oncol. 2023;24(5):457–67.
17. Nguyen HG, et al. First-in-human evaluation of a prostate-specific membrane antigen–targeted near-infrared fluorescent small molecule for fluorescence-based identification of prostate cancer in patients with high-risk prostate cancer undergoing robotic-assisted prostatectomy. Eur Uroly Oncol. 2023. https://doi.org/10.1016/j.euo.2023.07.004.
18. Grimm J. Cerenkov luminescence imaging. In: Imaging and Visualization in the Modern Operating Room. Springer; 2015.
19. Thorek D, et al. Cerenkov imaging — a new modality for molecular imaging. Am J Nucl Med Mol Imaging. 2012;2(2):163–73.
20. Shaffer TM, Pratt EC, Grimm J. Utilizing the power of Cerenkov light with nanotechnology. Nat Nanotechnol. 2017;12(2):106–17.
21. Mc Larney B, Skubal M, Grimm J. A review of recent and emerging approaches for the clinical application of Cerenkov luminescence imaging. Front Phys. 2021;9. https://doi.org/10.3389/fphy.2021.684196.
22. Ciarrocchi E, Belcari N. Cerenkov luminescence imaging: physics principles and potential applications in biomedical sciences. EJNMMI Phys. 2017;4(1):1–31.
23. Das S, Thorek DLJ, Grimm J. Cerenkov Imaging. 2014, Elsevier. p. 213–234.
24. Mc Larney BE, et al. Detection of shortwave-infrared Cerenkov luminescence from medical isotopes. J Nucl Med. 2023;64(1):177–82.
25. Wang X, et al. Cherenkov luminescence in tumor diagnosis and treatment: a review. Photonics. 2022;9(6):390.
26. Robertson R, et al. Optical imaging of Cerenkov light generation from positron-emitting radiotracers. Phys Med Biol. 2009;54(16):N355–65.
27. Holland JP, et al. Intraoperative imaging of positron emission tomographic radiotracers using Cerenkov luminescence emissions. Mol Imaging. 2011;10(3):177–86, 1–3.
28. Spinelli AE, Ferdeghini M, Cavedon C, Zivelonghi E, Calandrino R, Fenzi A, et al. First human Cerenkography. J Biomed Optics. 2013;18(2):020502.
29. Thorek DLJ, Riedl CC, Grimm J. Clinical Cerenkov luminescence imaging of¹⁸F-FDG. J Nucl Med. 2014;55(1):95–8.
30. Pratt EC, et al. Prospective testing of clinical Cerenkov luminescence imaging against standard-of-care nuclear imaging for tumour location. Nat Biomed Eng. 2022;6(5):559–68.

31. Hu H, et al. Feasibility study of novel endoscopic Cerenkov luminescence imaging system in detecting and quantifying gastrointestinal disease: first human results. Eur Radiol. 2015;25(6):1814–22.
32. Spinelli AE, Schiariti MP, Grana CM, Ferrari M, Cremonesi M, Boschi F. Cerenkov and radioluminescence imaging of brain tumor specimens during neurosurgery. J Biomed Optics. 2016;21(5):050502. https://doi.org/10.1117/1.JBO.21.5.050502.
33. Grootendorst MR, et al. Intraoperative assessment of tumor resection margins in breast-conserving surgery using ¹⁸F-FDG Cerenkov luminescence imaging: a first-in-human feasibility study. J Nucl Med. 2017;58(6):891–8.
34. Grootendorst MR, et al. P094. Clinical feasibility of Cerenkov luminescence imaging (CLI) for intraoperative assessment of tumour excision margins and sentinel lymph node metastases in breast-conserving surgery. Eur J Surg Oncol (EJSO). 2015;41(6):S53. https://doi.org/10.1016/j.ejso.2015.03.132.
35. Michel C, et al. P7. Intra-operative margin detection using Cerenkov luminescence imaging during radical prostatectomy — initial results from the PRIME study. Eur J Surg Oncol (EJSO). 2015;41(11):S271.
36. Heuvel JO, et al. Cerenkov luminescence imaging in prostate cancer: not the only light that shines. J Nucl Med. 2022;63(1):29–35.
37. Costa PF, et al. ¹⁸F-PSMA Cerenkov luminescence and flexible autoradiography imaging in a prostate cancer mouse model and first results of a radical prostatectomy feasibility study in men. J Nucl Med. 2023;64(4):598–604.
38. Darr C, et al. First-in-man intraoperative Cerenkov luminescence imaging for oligometastatic prostate cancer using 68Ga-PSMA-11. Eur J Nucl Med Mol Imaging. 2020;47(13):3194–5.
39. Chen X, et al. Sensitivity improved Cerenkov luminescence endoscopy using optimal system parameters. Quant Imaging Med Surg. 2022;12(1):425–38.
40. Costa PF, et al. Radiation protection and occupational exposure on ⁶⁸Ga-PSMA-11–based Cerenkov luminescence imaging procedures in robot-assisted prostatectomy. J Nucl Med. 2022;63(9):1349–56.
41. Olde Heuvel J, et al. Performance evaluation of Cerenkov luminescence imaging: a comparison of 68Ga with 18F. EJNMMI Physics. 2019;6(17). https://doi.org/10.1186/s40658-019-0255-x.
42. Trotter J, et al. Positron emission tomography (PET)/computed tomography (CT) imaging in radiation therapy treatment planning: a review of PET imaging tracers and methods to incorporate PET/CT. Adv Radiat Oncol. 2023;8(5): 101212.
43. Heo Y-A. Flotufolastat F 18: Diagnostic first approval. Mol Diagn Ther. 2023;27(5):631–6.

Publisher's Note Springer Nature remains neutral with regard to jurisdictional claims in published maps and institutional affiliations.

Springer Nature or its licensor (e.g. a society or other partner) holds exclusive rights to this article under a publishing agreement with the author(s) or other rightsholder(s); author self-archiving of the accepted manuscript version of this article is solely governed by the terms of such publishing agreement and applicable law.